Advanced Steel Construction – Vol. 15 No. 4 (2019) 364–376
DOI:10.18057/IJASC.2019.15.4.7

MODELING THE LOCAL BUCKLING FAILURE OF ANGLE SECTIONS WITH BEAM ELEMENTS

Farshad Pourshargh[1], Frederic P. Legeron[2,4] and Sébastien Langlois[3,*]

1 Ph.D. candidate at Université de Sherbrooke, Sherbrooke, Canada
2 Eng., Ph.D. Formerly Professor, Civil Engineering Department, Université de Sherbrooke, Sherbrooke, Canada
3 Eng., Ph.D. Assistant professor, Civil Engineering Department, Université de Sherbrooke, Sherbrooke, Canada
4 Present affiliation: Vice President, Parsons, Dubai, UAE
**(Corresponding Author: Email address: Sebastien.Langlois@USherbrooke.ca)*

A B S T R A C T

Slender steel sections are widely used in the construction of steel structures such as lattice structures for transmission line and telecommunication towers. Local buckling may be the observed failure mode under compression loads for these slender sections, and many experimental studies have been conducted to evaluate their resistance. All steel design codes include equations to account for local buckling. In numerical models, local buckling can be reproduced using 2D shell or 3D elements. Nonlinear numerical models have been developed in the last decades that can capture the complex behavior of lattice structures up to failure. These models typically use beam elements that consider correctly the global buckling and yielding of sections but do not consider the local buckling of angles due to geometrical limitations. This article proposes a method that modifies the material behavior of sections to involve the local buckling failure in the analysis. Forty-two experimental tests were conducted on short angles and a general stress-strain formula was defined based on the test results. The formula relates the local buckling slenderness ratio of the members to a material constitutive law that accounts for the local buckling. To evaluate the method, the numerical results were compared to those of four x-braced frame configurations using slender angle sections. The results demonstrate that the proposed method can accurately model the local buckling failure of fiber beam elements.

ARTICLE HISTORY

Received: 11 January 2019
Revised: 26 February 2019
Accepted: 17 July 2019

K E Y W O R D S

Lattice steel tower;
Angle section;
Local buckling;
Finite element model;
Nonlinear behavior;
Fiber beam element

1. Introduction

Angle steel members are widely used in steel lattice structures for transmission lines and telecommunications. Lattice towers that are made of angle members exhibit complex structural behavior, which is mainly due to connection eccentricity, bolt slippage, local buckling and their impacts on failure modes. The standard procedure for designing tower members is to build a simple linear model of the structure for determining the forces in each member and to evaluate the resistance using design code equations. This type of analysis may not be correct because the buckling resistance should be verified as an integrated part of the design and not as an independent stage [1, 2]. To overcome the limitations of this simple analysis, transmission line lattice towers are typically tested under various load conditions in full-scale field tests prior to mass production.

Prasad Rao [3] reported that 32 towers out of 138 full-scale tests at the Structural Engineering Research Centre [CSIR-SERC] experienced various types of premature failures, which demonstrates the limitations of the design method that is used in practice. To study the failure in detail, they modeled three towers and analyzed them using the NE-Nastran nonlinear finite element software. The option for geometric and material nonlinearity in the software was used to obtain the behavior and limit loads. The entire tower was modeled using beam-column elements. However, to capture more details, the failed compression bracings were modeled as plate elements. The test failure pattern coincided with the analysis failure pattern for both beam and plate modeling. However, nonlinear finite element analysis predicted a failure load that was 7 to 14 percent higher than the test results.

Another study was performed by the same researchers [4] on five prematurely failed towers. They encountered overprediction of the strength by nonlinear analysis and concluded that finite element analysis is still not a fully reliable method for predicting tower strength and the tests remain necessary for this objective. However, it is indicated that the nonlinear analysis is essential for understanding the behavior, load carrying capacity, design deficiencies, and instability in the structure. This type of nonlinear model aims at capturing the complex and nonlinear behavior of steel lattice structures. It is not a practical design method because it does not rely on design code equations or more advanced methods such as the direct strength method (DSM) [5, 6, 7] to evaluate the resistance of sections. It provides a one-step numerical model for representing the pre- and post-buckling behaviors of the structure. This type of model is useful as an alternative or complement to full-scale tests for understanding the behavior and evaluating the resistance of lattice towers. Recent works showed that depending on the objective of the modeling, the following characteristics of lattice behavior might need to be considered: joint eccentricity [8, 9], bolt slippage [10], and residual stresses [11], among others. However, in this type of model, which normally simulates the elastoplastic buckling of angle members, the potential local buckling of members is neglected. This article will focus on developing an efficient method to account for local buckling in nonlinear models of lattice structures.

Currently, most research on the modeling of angle members uses either beam elements or 2D shell elements. Angle sections may undergo global or local buckling instability under a compression load, depending on the slenderness and the width-to-thickness ratios. Shell elements can represent the full three-dimensional behavior of angle sections and local buckling with high accuracy if the mesh is sufficiently refined. However, for large and complex structures such as lattice towers, the high number of members render the use of shell elements impractical. For example, Shan et al. [12], proposed modeling angle members by nonlinear plate elements. They included both material and geometric nonlinearities in the study; however, the analysis procedure was computation-intensive and time-consuming. They concluded that 2D elements can only be used for small structures and as a research tool. This conclusion has been supported by other researchers [13]. In slender angle sections with a high width-to-thickness ratio, the global buckling deformation is accompanied by local buckling of leg plates [14] and this effect should be incorporated into the finite element model of the structure. Lee and McClure [13] developed an L-section beam finite element for elastoplastic large deformation analysis. In terms of the computational time, the beam element is 2.4 times more efficient than shell modeling if the member length is equal to 4 meters.

The fiber beam element is a highly effective element that is used with success to model angle sections. This element can properly incorporate the stress and yielding effects in the member. Kitipornchai et al. [19, 20] reported an analysis with nonlinear fiber elements of angle sections under axial and bending loads. Numerical studies were conducted on various structures and the angle members were modeled as fiber elements. Several examples were presented to demonstrate the satisfactory performance of the fiber element model in predicting the ultimate behavior of imperfect angle columns. The results that were obtained from the study were compared to experimental tests on two pairs of angle trusses with web members.

Vieira et al. [21] and Carrera et al. [22] proposed a 1D beam element for modeling the buckling of beams using analytical formulas. The results accorded with finite element models. Several limitations in capturing the local buckling behavior were reported. According to the authors, additional tests and experiments are needed for extending the method.

Other computational methods for calculating the buckling loads of thin-walled sections were studied. Huang et al. [23] developed a mathematical formulation. They considered the angle section as an example and conducted a numerical analysis of the elastic and inelastic buckling using finite element models. The results from beam and shell elements were compared with the theoretical results. It was concluded that the mathematical solution of higher order differential equations is complicated and for members with complicated deflections another method should be applied. Considering other research and experiments in this field, the approach with fiber elements is well adapted analytically for modeling the transmission tower structures; however, a full local buckling behavior that covers the pre- and post-buckling behaviors is not well defined.

The objective of this paper is to propose a method for incorporating the local buckling behavior in the finite element model of structures using fiber beam elements by developing a stress-strain behavior curve of steel. Forty-two slender section angle members were tested and full force-deflection curves were extracted. Then, a local buckling slenderness ratio was defined via the direct strength method [5] and equations were developed to relate the slenderness ratio to two specified points on the stress-strain curve. Considering these two points, full stress-strain equations were defined by using curve fitting techniques to model the compressive behavior of a slender angle with a specified slenderness ratio. Finally, the proposed method was evaluated by comparing its results to the test results on four full-scale X-braced frames of angle slender members that were obtained by Morissette [24].

2. Short angle specimens

2.1. Local buckling slenderness

The experimental program consists of testing 42 short angle members under pure compression. These tests were conducted to evaluate the global stress-strain behavior of angles that are failing due to local buckling. To characterize the sections that are undergoing local buckling, Table 1 introduces the local buckling slenderness ratio, which is denoted as λ_p and is defined in Equation 1. This ratio is used in the direct strength method [31] and was found to be useful for relating the properties of the angle to the stress-strain behavior.

$$\lambda_p = \sqrt{\frac{F_y}{\sigma_{cr}}} \tag{1}$$

In this equation, F_y stands for the yielding stress of steel and σ_{cr} is the critical elastic local buckling stress for the member, which can be calculated using finite element software such as Code_Aster, ANSYS or ABAQUS. In this study, a finite strip software, namely, CUFSM, which is developed by Schafer [32], will be used to perform critical elastic buckling load calculations. CUFSM, which has been developed to accompany the direct strength method, is a finite strip elastic buckling analysis application. In the first step, the geometry of the member is modeled either manually or using a built-in cross-section library. Then, general end boundary conditions and loading are applied to the member and the section is meshed automatically with finite strips. Finally, the analysis provides the buckling mode shapes of the member and the critical elastic buckling load for each mode. This software is freely available.

In practice, FE analysis is time-consuming for engineers. However, as a simplification, a mathematical relation can be developed between the local buckling stress and the width-to-thickness ratio b/t, where b is the width of the angle leg and t is the thickness of the leg. Based on all the angle members that are reported in Table 1, a formula is presented that relates σ_{cr} and ratio (b/t):

$$\left(\frac{b}{t}\right) = \frac{\alpha}{\sqrt{\sigma_{cr}}} \tag{2}$$

where the value of α is calculated to be 323 according to the curve fitting analysis that is shown in Fig. 1. In this work, the modulus of elasticity of steel was assumed to be 200,000 MPa. This simplification can be used when the boundary conditions of the angle member are fixed translation and free rotation. However, as shown in Fig. 1, the discrepancy in the local buckling stress can be important, especially at low b/t values. Therefore, for higher precision, the full procedure that is presented in the next sections, which involves a finite element model, is recommended.

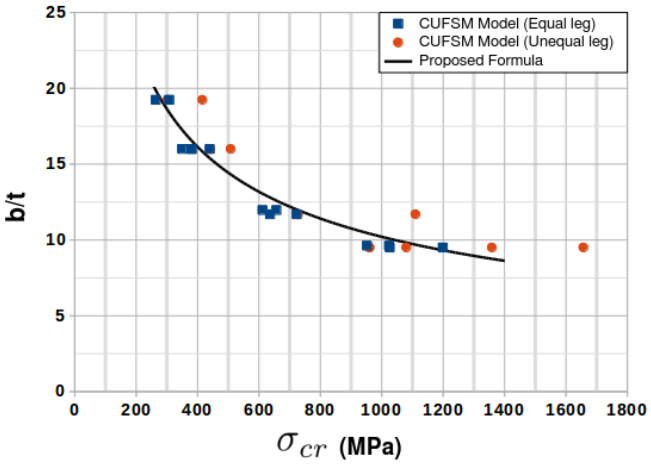

Fig.1 Calculated curve that relates σ_{cr} and (b/t) values

2.2. Experimental program

The objective of the experimental program is to provide test results on local buckling behavior from specimens of various geometries. Forty-two short angle specimens, which are listed in Table 1, were tested under pure compression and the force-deformation behavior was measured. The leg width-to-thickness ratio, namely, (b/t), of the specimens ranged from 9.5 to 19. According to (CSA-S16) [25] and Eurocode 3 [27], all specimens are classified as class 4 sections, which are subject to local buckling prior to yielding under compression. The steel grade of the specimens is ASTM-A36 [28] and their material properties are listed in Table 1.

The lengths of specimens were selected to avoid global buckling instability. Most configurations were tested on two identical specimens to evaluate the repeatability of results. The average result of these identical tests was considered the final result to better represent the types of sections that are available in the market. Since the specimens are short and they fail under the local buckling mode, the effects of geometrical imperfections and residual stresses are not considered. These effects are more important on global buckling mode, which is outside the scope of this article. Taking the discussed effects in consideration adds additional parameters to the prediction, which renders finding a solution highly complicated; hence, these effects are not investigated further in this article.

To provide continuous and uniform end conditions throughout the tests, the extremities of all specimens were accurately milled flat and strictly perpendicular to the axis of the angle. The specimens were supported by a thick steel plate without a hinge for the test. The alignment of the centroid of the angle with the line of action of the force was secured by top and bottom adjustment plates (Fig. 2) that were bolted to the thick plates. To avoid any eccentric moment, the center of the force that was applied by the machine coincided with the center of gravity of the section. The angle-shaped opening in each set of adjustment plates provided the required end constraints: fixed translation and free rotation.

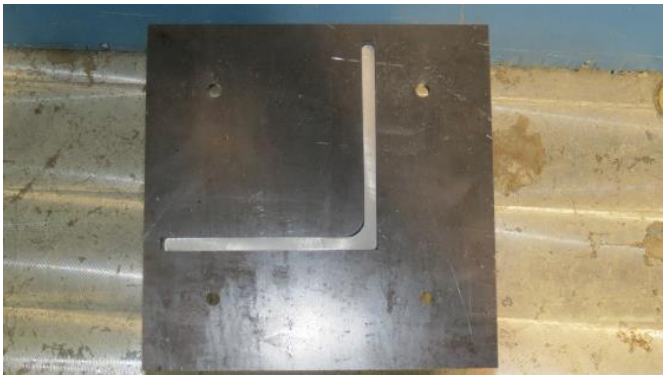

Fig. 2 Adjustment plate in the supports

Table 1
Properties of the short angle test specimens

Test	Section	Length (mm)	b/t	F_y (MPa)	F_u (MPa)	E (MPa)	σ_{cr} (MPa)	λ_p
1	L152x152x7.9	600	19.2	339	519	178000	264	1.13
2	L152x152x7.9	600	19.2	339	519	178000	264	1.13
3	L152x152x7.9	400	19.2	339	519	178000	308	1.05
4	L152x152x7.9	400	19.2	339	519	178000	308	1.05
5	L152x152x9.5	600	16	390	543	207000	381	1.01
6	L152x152x9.5	600	16	390	543	207000	381	1.01
7	L152x152x9.5	400	16	390	543	207000	440	0.94
8	L152x152x9.5	400	16	390	543	207000	440	0.94
9	L152x152x16	600	9.5	395	514	188281	1026	0.62
10	L152x152x16	600	9.5	395	514	188281	1026	0.62
11	L152x152x16	400	9.5	395	514	188281	1199	0.57
12	L152x152x16	400	9.5	395	514	188281	1199	0.57
13	L152X102X9.5	433	16	373	495	206297	508	0.86
14	L152X102X9.5	437	16	373	495	206297	508	0.86
15	L152X102X16	438	9.5	375	564	212700	1359	0.53
16	L152X102X16	439	9.5	375	564	212700	1359	0.53
17	L152X102X16	680	9.5	375	564	212700	1080	0.59
18	L152x152x9.5	598	16	392	541	201000	381	1.01
19	L152x152x9.5	597	16	392	541	201000	381	1.01
20	L152x152x9.5	598	16	392	541	201000	381	1.01
21	L152X102X9.5	718	16	371	492	208000	440	0.92
22	L152x152x9.5	850	16	380	526	210000	350	1.04
23	L152X102X16	800	9.5	375	563	212700	960	0.63
24	L152X102X16	300	9.5	375	563	212700	1657	0.48
25	L152X102X16	800	9.5	375	563	212700	960	0.63
26	L152x152x13	850	11.7	388	547	202626	636	0.78
27	L152x152x13	850	11.7	388	547	202626	636	0.78
28	L152x152x13	500	11.7	388	547	202626	723	0.73
29	L152x102x13	800	11.7	407	587	193387	727	0.75
30	L152x102x13	800	11.7	407	587	193387	727	0.75
31	L152x102x13	300	11.7	407	587	193387	1110	0.61
32	L152x102x7.9	800	19.2	405	557	204017	302	1.16
33	L152x102x7.9	800	19.2	405	557	204017	302	1.16
34	L152x102x7.9	300	19.2	405	557	204017	416	0.99

35	L76x76x6.35	400	12	379	526	203000	612	0.79
36	L76x76x6.35	400	12	379	526	203000	612	0.79
37	L76x76x6.35	300	12	379	526	203000	657	0.76
38	L76x76x6.35	300	12	379	526	203000	657	0.76
39	L76x76x7.9	400	9.6	388	555	203000	952	0.64
40	L76x76x7.9	400	9.6	388	555	203000	952	0.64
41	L76x76x7.9	300	9.6	388	555	203000	1024	0.62
42	L76x76x7.9	300	9.6	388	555	203000	1024	0.62

The compression jig was set up for performing the tests as shown in Fig. 3 in a 500-kN hydraulic testing machine. The loading was displacement-controlled at rates that ranged from 0.12 to 0.3 mm/min according to the length of the specimen to reach the maximum load within 5 to 10 minutes. The test was continued up to the occurrence of a substantial nonlinear behavior. The relative displacement of the specimens was measured by a displacement transducer that was attached to the adjustment plate from the bottom to the top (Fig. 3).

2.3. Material property tests

Two or three coupons were cut and prepared from each batch of steel material and tested under tension according to the ASTM A370-02 [29] standard. The values of F_y that were provided by the coupon tests were used to calculate λ_p for each specimen. The values are listed in Table 1.

3. Definition of material stress-strain behavior

Based on the force-deflection results from the short angle tests, 42 stress-strain material behaviors were extracted. Each material behavior is related to the corresponding λ_p value of the specimen. The values of σ(stress) and ε(strain) are calculated by assuming homogeneous behavior as σ = P/A and ε = δ/L, where P is the applied force (N); A is the cross-sectional area (mm^2); δ is the vertical deflection of the specimen (mm); and L is the length of the specimen (mm).

Fig. 4 plots the measured behaviors of six specimens. To characterize the behavior of a member under compression, it is assumed that the full stress-strain curve can be characterized by 2 points: A(ε_A,σ_A), which denotes the first peak in the curve, and B(0.01,σ_B). Table 2 reports the ε_A, σ_A, and σ_B values. Other points were also considered; however, based on the accuracy of the fitted curve, the two points that are specified above were selected. Using the short angle test results (Table 2) and a curve fitting technique, Equations 3 to 5 were developed for calculating the coordinates of points A and B based on the value of λ_p. Since the number of tested specimens was limited, the range of values of λ_p for which the equations apply was limited to 0.57-1.20. This also affected the calculated values of σ_A in terms of the material yield stress. Fig. 5 plots the equations and the distribution of the test points.

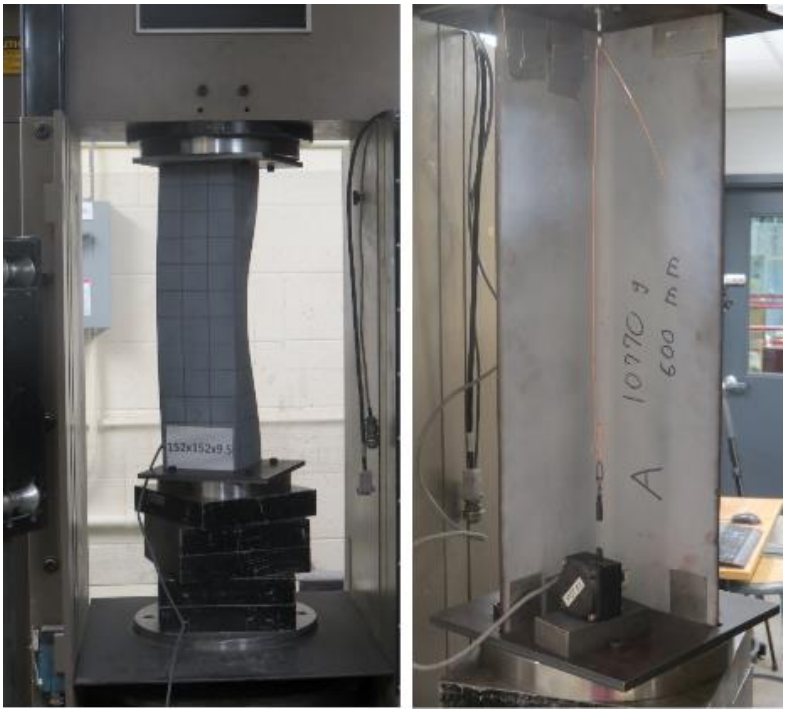

Fig. 3 Test setup and displacement transducer

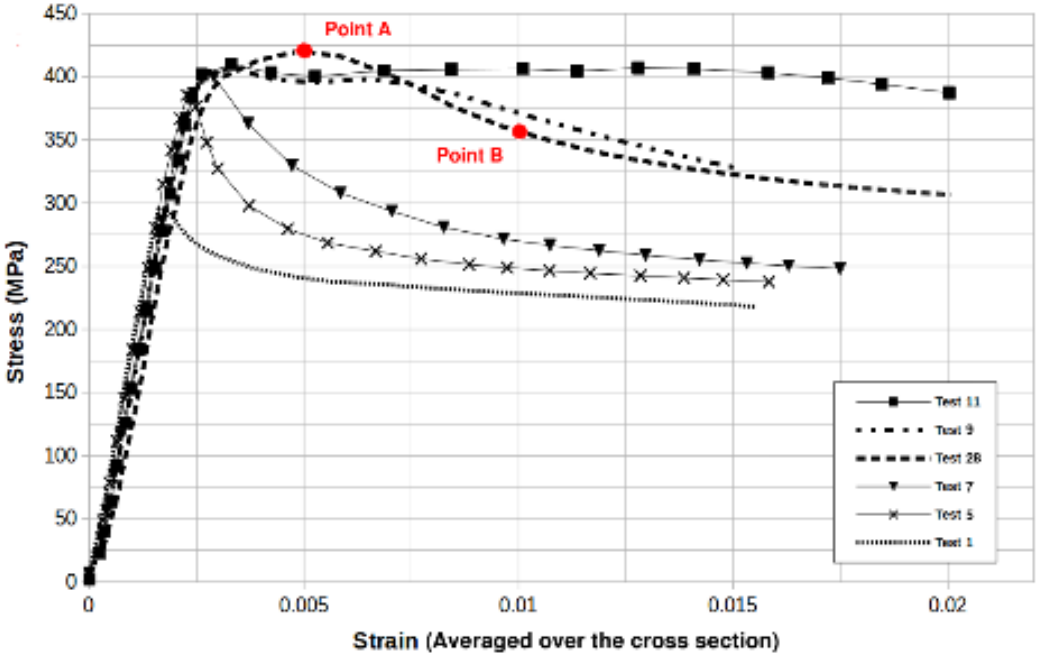

Fig. 4 Measured stress-strain behaviors of six test specimens

$$\varepsilon_A = 0.0004965 \times (1 + {\lambda_p}^{-11.6})^{\frac{1}{5.8}} + 0.001521 \qquad 0.57 < \lambda_p < 1.20 \qquad (3)$$

$$\sigma_A = 407.9 \times (1 + \lambda_p^{20})^{-\frac{1}{10}} \qquad 0.57 < \lambda_p < 1.20 \qquad (4)$$

$$\sigma_B = 350.1 \times {\lambda_p}^2 - 903.9 \times \lambda_p + 809.1 \qquad 0.57 < \lambda_p < 1.20 \qquad (5)$$

Table 2
Results of the short angle tests

Test	λ_p	ε_A	σ_A (MPa)	σ_B (MPa)
1	1.13	0.0017	298	228
2	1.13	0.0018	288	229.9
3	1.05	0.0022	313	234
4	1.05	0.0035	297	242
5	1.01	0.0023	389	248
6	1.01	0.0021	379	250
7	0.94	0.0028	401	269.7
8	0.94	0.0028	400	267.8
9	0.62	0.0032	407	371.2
10	0.62	0.0027	406	398.7
11	0.57	0.0032	409	406.6
12	0.57	0.0032	410	406.3
13	0.86	0.0029	367	271.7
14	0.86	0.0031	367	270.8
15	0.53	0.0035	350	374
16	0.53	0.0049	353	376
17	0.59	0.0022	350	350.7
18	1.01	0.0025	390	256.9
19	1.01	0.0026	384	254.8

20	1.01	0.0024	377	256.2
21	0.92	0.0024	371	254
22	1.04	0.0022	356	241.6
23	0.63	0.003	422	376
24	0.48	0.005	423	436.7
25	0.63	0.0035	425	392
26	0.78	0.0034	413	305
27	0.78	0.0032	413	301.8
28	0.73	0.0048	420	356.8
29	0.75	0.0036	414	332.2
30	0.75	0.0035	413	334
31	0.61	0.007	450	453
32	1.16	0.0021	336	234.6
33	1.16	0.0021	319	245.1
34	0.99	0.0031	404	285.7
35	0.79	0.0029	418	292.6
36	0.79	0.003	419	293
37	0.76	0.0034	411	329
38	0.76	0.0038	415	324.3
39	0.64	0.0031	431	406.8
40	0.64	0.0027	429	422
41	0.62	0.003	432	427
42	0.62	0.0031	429	423.6

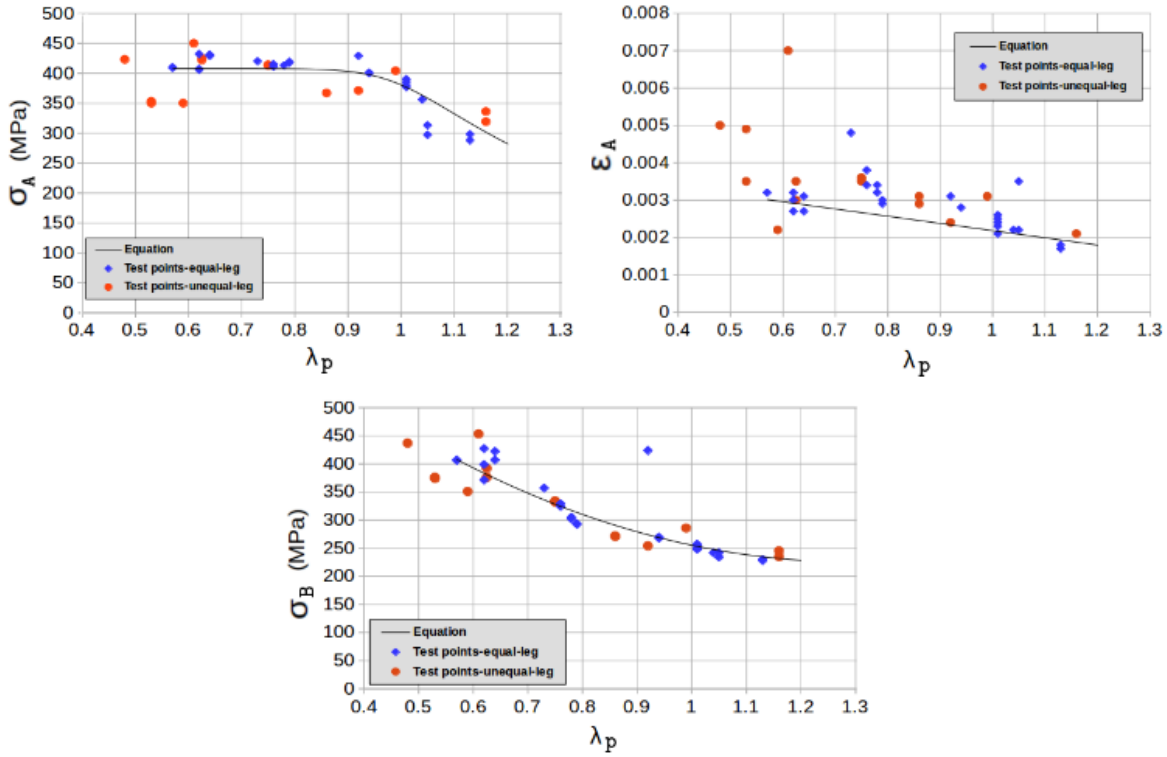

Fig. 5 Plots of equations 3 to 5 and the distribution of the test points

The coordinates of points A and B are used to calculate the three unknown parameters (C, D, and k) that are used to define the stress-strain equation (6). Since the behavior of steel in the first steps of loading is completely elastic, the third criterion that is used to calculate the parameters of the equation is the slope of standard steel stress-strain material in elastic range, which is assumed to be 200,000 MPa (Young's modulus). The main stress-strain equation is expressed as follows:

$$\sigma = \begin{cases} 200000 \times \varepsilon & \varepsilon \leq 0.0005 \\ C \times \varepsilon_m \times (\varepsilon_m + D \times \varepsilon_m{}^{(-k)})^{(-k)} & \varepsilon > 0.0005 \end{cases} \quad (6)$$

$$\varepsilon_m = 1000 \times \varepsilon \quad (7)$$

Equations 3 to 5 relate the λ_p value of any class 4 member to two characteristic points, namely, A and B, of the stress-strain curve. Then, Equation 6 relates these two points to a complete and modified stress-strain curve that can be included in a beam element as a material behavior. The values of the unknown parameters in the equation (C, D, and k) were obtained via trial and error. A simple script was developed for inputting the λ_p value. The script calculates the coordinates of points A and B based on Equations 3 to 5. Then, points A and B are substituted into Equation 6, which yields the full stress-strain behavior. Table 3 lists the values of parameters C, D and k that are calculated based on points A and B for each specimen and λ_p value. The output of Equation 6 can be entered as a nonlinear material behavior into any finite element software. An alternative simplified solution is to define the material as a bilinear stress-strain relation without using Equation 6. The bilinear behavior could be defined by using σ_A as F_y and the slope of the line that connect points A and B (AB) as E_t (the tangent modulus of the material). Fig. 6 compares the stress-strain curve that was calculated via Equation 6 with the test results from short angle specimens for six λ_p values.

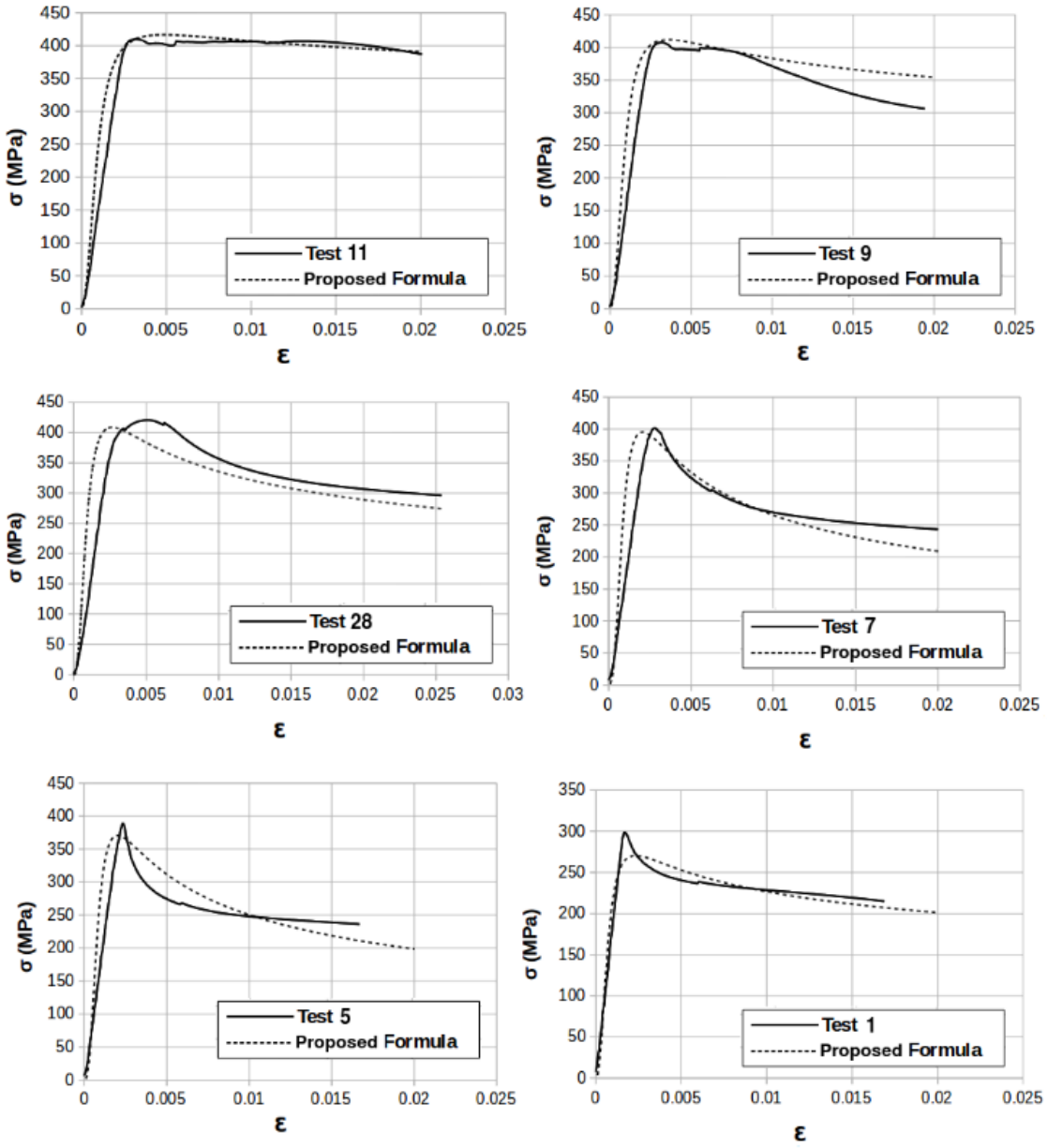

Fig. 6 Comparison of the stress-strain relationship between the test results and Equation 6

Table 3
Calculated values of parameters for Equation 6

Tests	λ_p	C	D	k
1,2	1.13	440.289	0.563	1.272
3,4	1.05	526.022	0.625	1.329
5, 6, 18, 19, 20	1.01	563.891	0.653	1.346
7, 8	0.94	601.782	0.692	1.349
9, 10	0.62	512.091	0.831	1.123
11, 12	0.57	479.906	0.844	1.068
13, 14	0.86	602.713	0.729	1.315
15, 16	0.53	449.86	0.848	1.018
17	0.59	493.722	0.84	1.091
21	0.92	605.266	0.702	1.343
22	1.04	536.673	0.633	1.334
23, 25	0.63	517.363	0.827	1.133
24	0.48	441.128	0.847	1.004
26, 27	0.78	583.226	0.764	1.263
28	0.73	565.003	0.786	1.224
29, 30	0.75	572.487	0.777	1.24
31	0.61	506.351	0.834	1.113
32, 33	1.16	409.118	0.538	1.246
34	0.99	578.983	0.665	1.351
35, 36	0.79	585.562	0.76	1.269
37, 38	0.76	575.722	0.773	1.247
39, 40	0.64	523.266	0.824	1.143
41, 42	0.62	512.091	0.831	1.123

According to Fig. 6, the calculated curves are comparable to the experimental results and they have an acceptable accuracy. This is also demonstrated in Table 4, which compares the values of ε_A, σ_A and σ_B from Equation 6 and experimental work on short angles. The mean value of the differences is very close to 1.0 and the COV values are reasonable for parameters σ_A and σ_B. The strain at the peak is always difficult to capture in angles showing close to elasto-perfectly plastic behavior. As a consequence, the COV value for parameter ε_A is relatively high. Despite the statistical comparisons in Table 4, the trend of the stress-strain curve that was calculated via the formula accords with the experimental results and the inaccuracy of ε_A does not impact the close agreement of the predicted curve with the experimental results.

Table 4
Comparison of parameters that were calculated via Equation 6 with test values for parameters ε_A, σ_A, and σ_B

Test	ε_A (T)	σ_A (T)	σ_B (T)	ε_A (F)	σ_A (F)	σ_B (F)	ε_A (F/T)	σ_A (F/T)	σ_B (F/T)
1	0.0017	298	228	0.0021	317	234	1.24	1.06	1.03
2	0.0018	288	230	0.0021	317	234	1.17	1.1	1.02
3	0.0022	313	234	0.002	358	245	0.91	1.14	1.05
4	0.0035	297	242	0.002	358	245	0.57	1.21	1.01
5	0.0023	389	248	0.002	376	252	0.87	0.97	1.02
6	0.0021	379	250	0.002	376	252	0.95	0.99	1.01
7	0.0028	401	270	0.0019	397	269	0.68	0.99	1
8	0.0028	400	268	0.0019	397	269	0.68	0.99	1
9	0.0032	407	371	0.0036	412	383	1.13	1.01	1.03
10	0.0027	406	399	0.0036	412	383	1.33	1.01	0.96
11	0.0032	409	407	0.0046	416	402	1.44	1.02	0.99
12	0.0032	410	406	0.0046	416	402	1.44	1.01	0.99
13	0.0029	367	272	0.0022	406	291	0.76	1.11	1.07

14	0.0031	367	271	0.0022	406	291	0.71	1.11	1.07
15	0.0035	350	374	0.0042	418	428	1.2	1.2	1.14
16	0.0049	353	376	0.0042	418	428	0.86	1.19	1.14
17	0.0022	350	351	0.0042	414	397	1.91	1.18	1.13
18	0.0025	390	257	0.002	373	251	0.8	0.96	0.98
19	0.0026	384	255	0.002	376	252	0.77	0.98	0.99
20	0.0024	377	256	0.002	376	252	0.83	1	0.98
21	0.0024	371	254	0.0021	401	274	0.88	1.08	1.08
22	0.0022	356	242	0.0019	363	247	0.86	1.02	1.02
23	0.003	422	376	0.0034	411	379	1.13	0.97	1.01
24	0.005	423	437	0.0046	421	433	0.92	1	0.99
25	0.0035	425	392	0.0034	411	379	0.97	0.97	0.97
26	0.0034	413	305	0.0024	408	317	0.71	0.99	1.04
27	0.0032	413	302	0.0024	408	317	0.75	0.99	1.05
28	0.0048	420	357	0.0026	409	336	0.54	0.97	0.94
29	0.0036	414	332	0.0025	408	328	0.69	0.99	0.99
30	0.0035	413	334	0.0025	408	328	0.71	0.99	0.98
31	0.007	450	453	0.0038	412	388	0.54	0.92	0.86
32	0.0021	336	235	0.0021	302	231	1	0.9	0.98
33	0.0021	319	245	0.0021	302	231	1	0.95	0.94
34	0.0031	404	286	0.002	384	257	0.65	0.95	0.9
35	0.0029	418	293	0.0024	408	314	0.83	0.98	1.07
36	0.003	419	293	0.0024	408	314	0.8	0.97	1.07
37	0.0034	411	329	0.0025	408	323	0.74	0.99	0.98
38	0.0038	415	324	0.0025	408	323	0.66	0.98	1
39	0.0031	431	407	0.0033	411	374	1.06	0.95	0.92
40	0.0027	429	422	0.0033	411	374	1.22	0.96	0.89
41	0.003	432	427	0.0036	412	383	1.2	0.95	0.9
42	0.0031	429	424	0.0036	412	383	1.16	0.96	0.9
Average							0.93	1.02	1
COV (%)							30.29	7.56	6.53

Note: (T: Test, F: Formula) – The stress values are specified in MPa.

4. Evaluating the method with experimental results

4.1. Experimental Program

To evaluate the accuracy of the method, the numerical results were compared to the results of experimental tests that were performed at Université de Sherbrooke [24] on four X-bracing frame configurations. The test setup is a two-dimensional frame than can include angle members that act as X-braces. Fig. 7 and Fig. 8 present a sketch and a photograph of the test set-up. A lateral load was applied to the frame, which introduces compression and tension forces into the angles. The maximum capacity of the jack is 500 kN and it is mounted horizontally to a rigid supporting system. The frame was restrained by steel cables to avoid out-of-plane deflections. The beam-to-column connections were designed as pinned joints using a single bolt such that no bending moment was applied to the frame members and the lateral force induced direct axial tension and compression into the angles.

To measure the applied force to the angles, strain gauges were placed on end connection plates. Fig. 9 presents the geometry of the end plates. The end plates were of thickness 25.4 mm and two sets of plates were prepared for bolt sizes of 12.7 mm and 15.9 mm. To ensure the accuracy of the measured force, all assemblies of end plates and strain gauges were calibrated separately. Then, the recorded data from the strain gauges that were mounted on the end plates could be transformed to the applied force. In addition, displacement transducers were used to measure the lateral and out-of-plane deformations of the frame and braces. The load was applied based on the displacement control principle with a rate of 0.5 mm/min.

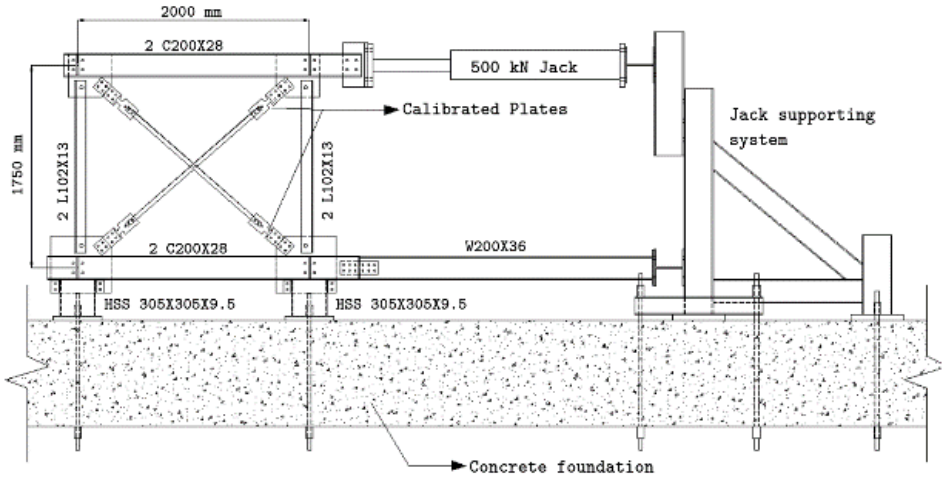

Fig. 7 Schematics of the test setup [24]

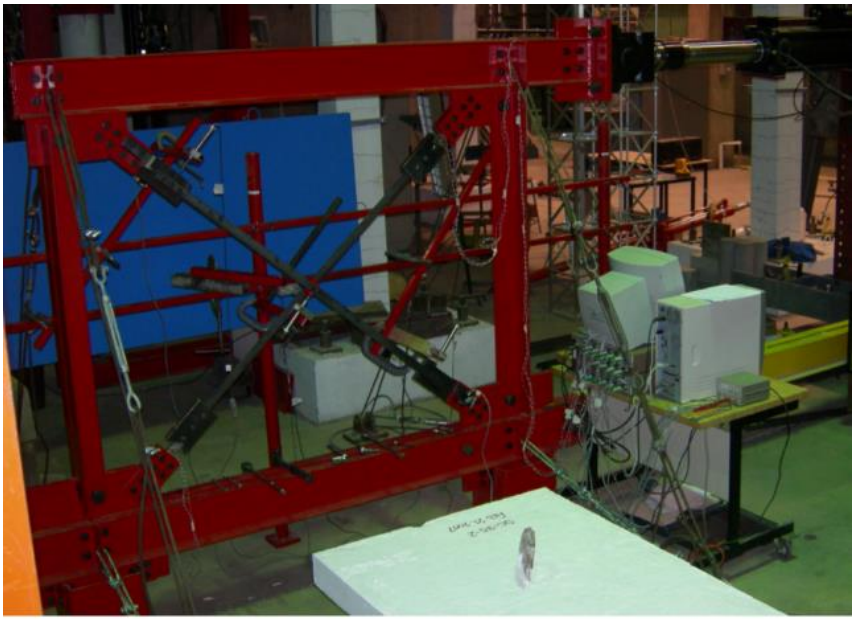

Fig. 8 X-bracing test setup [24]

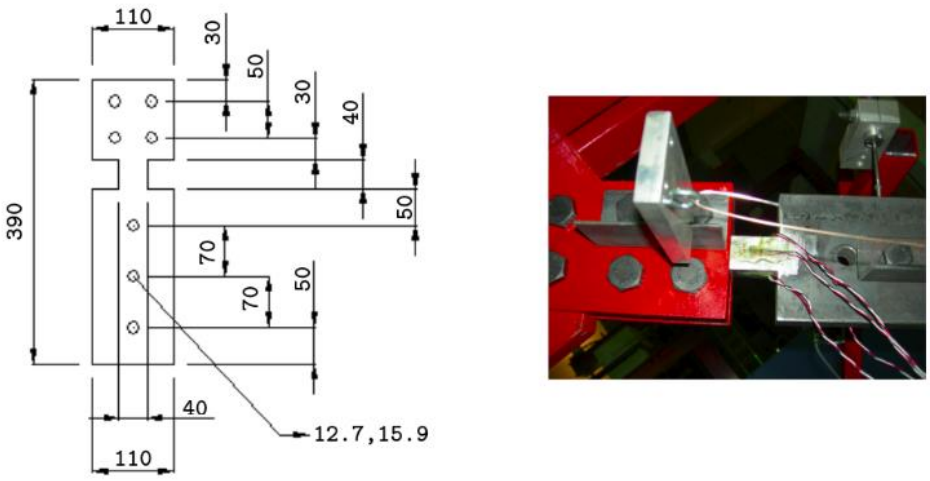

Fig. 9 Geometry of the end plates and locations of the strain gauges (dimensions in millimeters) [24]

4.2. Test Specimens

The X-bracing configuration involves two single angle sections under tension and compression. The target member is the angle under compression. Each angle is connected to the end plates using three bolts on one leg. The same leg is restrained in the middle of the member by a single bolt that is connected to the other bracing member, which is under tension. A filler plate was provided to fit the space between two angles in the middle and to ensure sufficient lateral support at the point of attachment (Fig. 10). The two configurations were L38X38X3.2 and L44X44X3.2 angle sections. The repeatability of results was assessed by testing two specimens for each configuration. Table 5 lists the specimens and their properties, which are based on tests that were conducted on coupons.

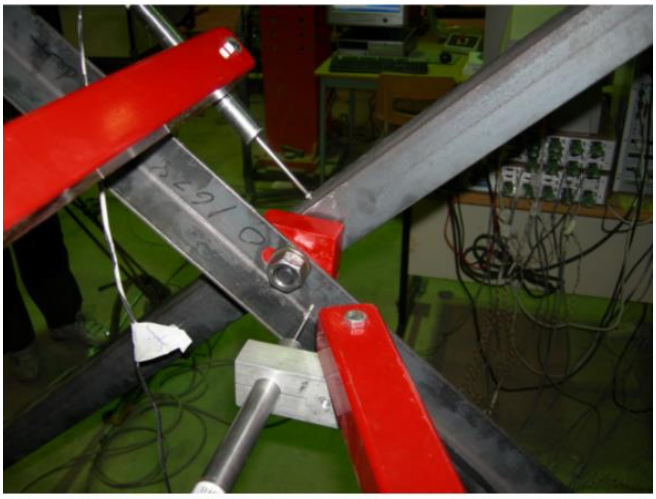

Fig. 10 Lateral support of the angles in the middle [24]

Table 5
Details of the X-bracing test specimens

Test	Section	D (mm)	F_y (MPa)
1	L38X38X3.2	12.7	370
2	L38X38X3.2	12.7	392
3	L44X44X3.2	15.9	393
4	L44X44X3.2	15.9	393

Note: (D: Bolt diameter)

4.3. Finite Element Modeling of the Specimens

The four angle specimens of the previous section were modeled using the Code_Aster software. Fiber beam elements are considered, and the optimum element size was evaluated to be 100 mm after conducting preliminary tests. To simplify the analysis, only the bracing angle members and the end connection plates are included in the model. A preliminary deflection value of Length/1000 [30] at the mid-length of the braces is applied to the weak bending axis as a global geometrical imperfection. It is assumed that the outside frame members are rigid in comparison to the angle members. Therefore, the end connection plates on top are supported by fixed supports with only unrestrained lateral displacement. The bottom supports are assumed to be fixed. The angle members are connected to these supports via two elements: a rigid beam element, which is used to include the member eccentricity, and a nonlinear spring, which is used to model the three-bolt-connection behavior. The properties of the spring element depend on the slippage and the bolted connection behavior according to the formulas that are presented by Rex et al. [33]. To model the single bolt that attaches the members at the middle of the bracing system, it is assumed that the middle nodes have identical displacement. However, the relative rotational displacement is free at this point.

The proposed method was applied to the analysis. First, σ_{cr} was calculated for each specimen using Code_Aster (Fig. 11). Since the boundary conditions of the members are not as described in Section 2.1, Equation 2 cannot be used and finite element modeling is implemented instead. In the X-bracing tests, the angle member needed to be restrained at the middle for modeling the pinned connection. Since CUFSM could not apply this type of restraint to the member, Code_Aster was used to perform the calculation. The bracing member under compression was modeled in Code_Aster using plate elements and mesh refinement was optimized via several trials. Each element had four corner nodes with six degrees of freedom and the maximum element size was 4 mm. Fixed boundary conditions were applied to the nodes on one leg of the member on each end. To model the constraint in the middle of the brace member, a hinged support was applied to a node on the same supported leg (Fig. 7). Then, the elastic buckling analysis was performed and the σ_{cr} value was calculated for the brace member.

The next step was to calculate the λ_p value for each specimen via Equation 1. Table 6 summarizes the calculated σ_{cr} and λ_p values for each specimen. Then, the stress-strain curve is calculated using the two steps that were specified earlier: first, Equations 3 to 5 were used to calculate two points, namely, A and B, on the curve for the specified value of λ_p; second, the parameters in Equations 6 and 7 were calculated such that the stress-strain curve passes through points A and B. In the final step, the calculated curve is applied as a material behavior to the fiber elements of the specimens. The nonlinear analysis phase is completed by Code_Aster and the assumptions of nonlinear material and large displacements are included in the procedure.

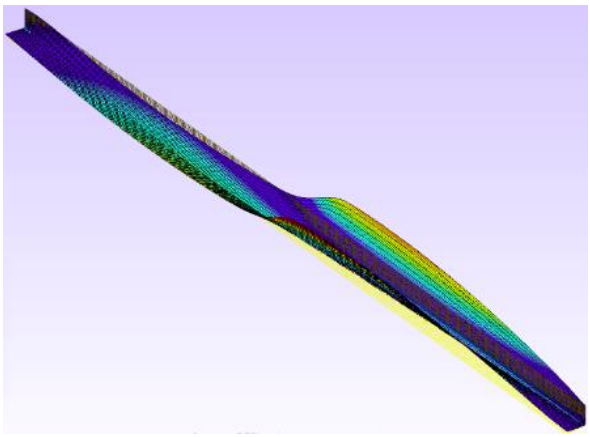

Fig. 11 Local buckling mode of a specimen (Test 3)

Table 6
Calculated σ_{cr} and λ_p values for the test specimens

Test	σ_{cr} (MPa)	λ_p
1	295	1.11
2	295	1.15
3	234	1.29
4	234	1.29

4.4. Results comparison and discussion

The experimental specimens failed due to local buckling phenomena. Fig. 12 shows the final deflection for four of the test specimens. Fig. 13 compares the failure stresses of the experimental tests to those of the finite element models and the member capacity based on ASCE 10-97 [34] and EC3 [27]. To evaluate the performance of the presented method, another set of analyses is performed without applying the proposed method to account for local buckling in the model. According to the comparisons, neglecting the local buckling failure in the analysis results in very high failure stresses. In the class

4 sections of this study, the local buckling failure controls the member capacity. Although the global buckling effect is included in the analysis due to large displacement option, it cannot take into account local failures which results in very high values of failure stress.

According to Table 7, the results of failure stress ($\sigma_{failure}$) for the finite element model are much more accurate and consistent with the tests when the presented method is applied. The mean value of FEA to Test results is 1.02 when the modification of material behavior is involved in the model. Despite the use of large displacement analysis, the above value increases dramatically to 1.54 if the effect of local buckling is ignored. Hence, the procedure that is presented in this study offers an appropriate solution for modeling the local buckling behavior of slender sections by beam elements.

Comparing the results of the presented method and the design capacity of the specimens that is based on ASCE 10-97 and EC3, the proposed method yields results that are similar to ASCE 10-97 and that are consistent with (but less conservative than) EC3. The coefficient of variation (COV) is slightly less than for design codes. For test 4, the discrepancy between the finite element model and the experimental test reaches a maximum of 15 percent. This is also consistent with the maximum error that is obtained with ASCE 10-97. This error could be due in part to the loading and boundary conditions that are used in the bracing tests, which are not perfectly represented in the model and in the codes.

Fig. 12 Local failure of test specimens (2 and 3) [24]

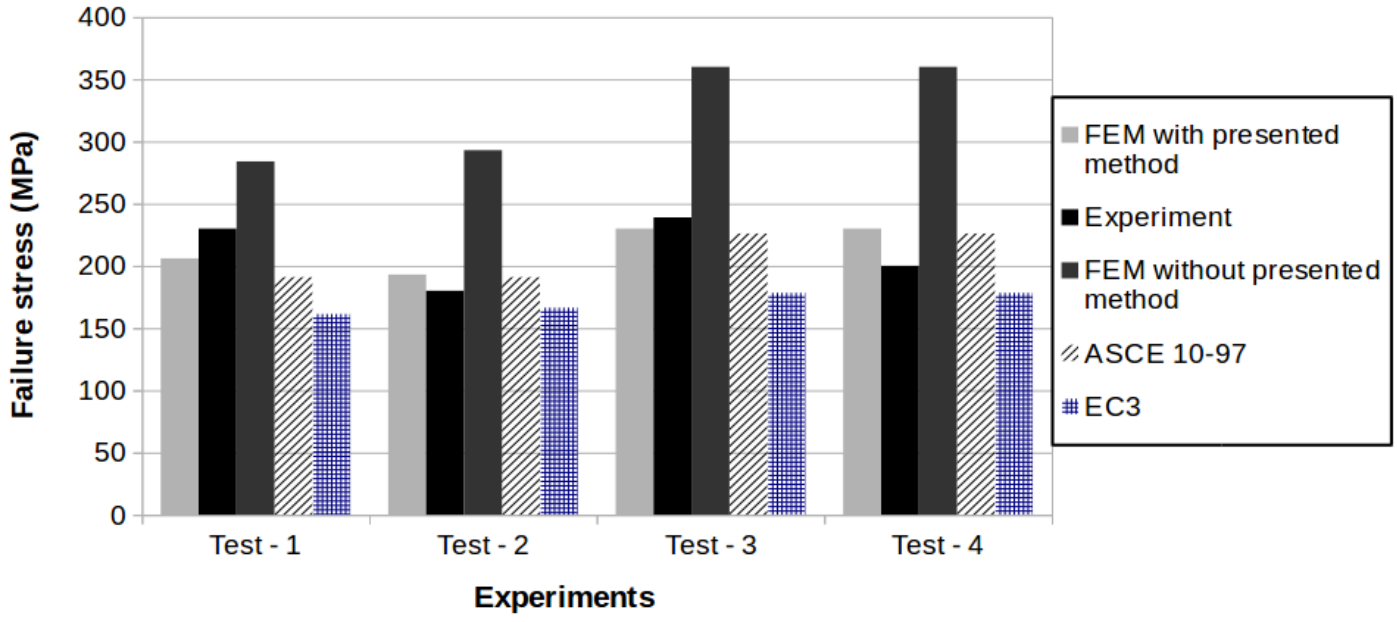

Fig. 13 Comparison of failure stress results

Table 7
Accuracy of the analysis with and without utilization of the presented method

Test	$\sigma_{failure}$ FEA (MPa)		$\sigma_{failure}$ test (MPa)	$\sigma_{capacity}$ ASCE (MPa)	$\sigma_{capacity}$ EC3 (MPa)	$\sigma_{failure}$ (FEA/test) ratio		ASCE / test	EC3/test
	w-lb	w/o-lb				w-lb	w/o-lb		
1	206	284	230	191	162	0.89	1.23	0.83	0.7
2	193	293	180	191	167	1.07	1.62	1.06	0.92
3	230	360	239	226	179	0.96	1.5	0.94	0.75
4	230	360	200	226	179	1.15	1.8	1.13	0.89
Average						1.02	1.54	0.99	0.82
COV (%)						11	15.4	13.2	13.3

Note: (w-lb: with local buckling and w/o-lb: without local buckling)

5. Conclusions

This article presented a new method for including the local buckling failure of class 4 members that are modeled by fiber beam finite elements. To consider this phenomenon, the stress-strain material behavior of the member was modified in the finite element model. A stress-strain curve formula was provided for each class 4 member that is based on the local buckling slenderness value (λ_p) of the member. Forty-two short angle specimens with λ_p values between 0.57 and 1.20 were tested and the force-deflection behavior of each specimen was recorded. Then, the stress-strain behavior was calculated for each of the λ_p values of the tests. Based on the above stress-strain behaviors and curve fitting technique, a general formula was presented that relates the λ_p value to a stress-strain material behavior.

To apply the method to a full-scale model, each class 4 member is recognized and the corresponding λ_p value is calculated. In the next step, the modified stress-strain curve is generated via the presented formula. Finally, the curve is assigned to the corresponding member as the material behavior in the finite element software.

To evaluate the feasibility and accuracy of the method, it was implemented for four cross-braced frame structures that were tested at Université de Sherbrooke. For the two studied configurations, class 4 angle sections were used as bracing members. The results were compared to two fiber element models, with and without using the proposed method. It was observed that when utilizing the proposed method in the models, the mean ratio of the model-to-test failure stress is 1.02, whereas this ratio increases to 1.54 when the method is not utilized. Additionally, comparing the proposed method to the design capacity that is calculated based on Eurocode and ASCE standards demonstrated that the new method provides more consistent results. Although the proposed method is not a practical design procedure, it may be used to improve nonlinear beam models of lattice towers that aim at complementing and reducing the need for full-scale transmission tower tests.

The presented method for modifying the material stress-strain behavior is only valid for the $\lambda_p$values interval of 0.57 to 1.20. Future research is needed for expanding this interval to cover more versatile class 4 sections such as unequal leg angles. Additionally, the method was validated with only four bracing tests. Further investigations should be conducted to validate the proposed method on more complex structures and field test results.

Acknowledgements

The authors gratefully acknowledge the financial support from the National Sciences and Engineering Research Council of Canada (NSERC), RTE and Hydro-Québec.

References

[1] Chan S. and Cho S., Second order analysis and design of angle trusses part i: Elastic analysis and design, Engineering Structures, 30, 616–625, 2008.
[2] Cho S. and Chan S., Second order analysis and design of angle trusses part ii: Plastic analysis and design, Engineering Structures, 30, 626–631, 2008.
[3] Prasad Rao, N. and Samuel K.G.M., Lakshmanan N. and Nagesh, R.I., Failure analysis of transmission line towers, Journal of Performance of Constructed Facilities, 25(3), 231–240, 2011.
[4] Prasad Rao N., Samuel K.G.M., Lakshmanan N., Nagesh R.I., Investigation of transmission line tower failures, Journal of Engineering Failure Analysis, 17, 1127–1141, 2010.
[5] Schafer B., Advances in direct strength design of thin-walled members, Advanced Structures, 1, 333–339, 2003.
[6] Silvestre N., Camotim D. and Dinis P.B., Post-buckling behaviour and direct strength design of lipped channel columns experiencing local/distortional interaction, Journal of Constructional Steel Research, 73, 12–30, 2012.
[7] Martins A.D., Camotim D. and Dinis P.B., On the distortional-global interaction in cold-formed steel columns: Relevance, post-buckling behaviour, strength and DSM design, Journal of Constructional Steel Research 145, 449–470, 2018.
[8] Bouchard P.-L., Calcul de la capacité de pylônes à treillis avec une approche stabilité. Mémoire de maîtrise. Université de Sherbrooke, 2013.
[9] Sad Saoud K., Langlois S., Loignon A. and Lamarche C.P., Failure analysis of transmission line steel lattice towers subjected to extreme loading. Annual Conference of the Canadian Society for Civil Engineering, June 13-16, Fredericton, Canada, 2018.
[10] Prasad Rao N., Samuel K.G.M., Lakshmanan N. and Nagesh R.I., Effect of bolt slip on tower deformation, Practice Periodical on Structural Design and Construction, 17(2), 65–73, 2012.
[11] Gravel G, Bouchard P.L., Prud'homme S., Sad Saoud K. and Langlois S., Assessment of the effect of residual stresses on the mechanical behavior of steel lattice transmission towers. Annual Conference of the Canadian Society for Civil Engineering, June 13-16, Fredericton, Canada, 2018.
[12] Shan L. and Peyrot A.H., Plate element modeling of steel angle members, Journal of Structural Engineering (ASCE), 114(4), 821–840, 1988.
[13] Lee P.-S. and McClure G., A general three-dimensional l-section beam finite element for elastoplastic large deformation analysis, Computers and Structures, 84, 215–229, 2006.
[14] Park Y.-S., Iwai S., Kameda H. and Nonaka T., Very low cycle failure process of steel angle members, Journal of structural engineering, 122(2), 133–141, 1996.
[15] Becque J. and Rasmussen K.J., Experimental investigation of local-overall interaction buckling of stainless steel lipped channel columns, Journal of Constructional Steel Research, 65(8-9), 1677–1684, 2009.
[16] Rasmussen K.J., Design of slender angle section beam-columns by the direct strength method, Journal of Structural Engineering, 132(2), 204–211, 2006.
[17] Haidarali M. and Nethercot D., Local and distortional buckling of cold-formed steel beams with edge-stiffened flanges, Journal of Constructional Steel Research, 73, 31–42, 2012.
[18] Haidarali M., Nethercot D. and Ashraf M., Local buckling of cold-formed steel lipped z section beams under pure bending, 5th International Conference on Advances in Steel Structures, ICASS 2007, 3, 474–480, 2007.
[19] Kitipornchai S. and Chan S., Nonlinear finite-element analysis of angle and tee beam-columns, Journal of Structural Engineering (ASCE), 113(4), 721–739, 1987.
[20] Kitipornchai S., Albermani F. and Chan S., Elastoplastic finite-element models for angle steel frames, Journal of Structural Engineering, (ASCE), 116 (10), 2567–2581, 1990.
[21] Vieira R.F., Virtuoso F.B.E., Pereira E.B.R., Buckling of thin-walled structures through a higher order beam model, Computers and Structures, 180, 104–116, 2017.
[22] Carrera E., Pagani A. and Petrolo M., Refined 1D Finite Elements for the Analysis of Secondary, Primary, and Complete Civil Engineering Structures, Journal of Structural Engineering, 141(4), 2015.
[23] Huang L., Li B. and Wang Y., Computation Analysis of Buckling Loads of Thin-Walled Members with Open Sections, Mathematical Problems in Engineering Volume 2016, Article ID 8320469.
[24] Morissette E., Évaluation des normes de calcul et du comportement des cornières simples en compression utilisées comme contreventements dans les pylônes à treillis en acier, Masters Degree Thesis, Université de Sherbrooke, 2008.
[25] Handbook of Steel Construction - Ninth Edition, Canadian Institute of Steel Construction - ISBN : 0-88811-114-2, 2006.
[26] Steel construction manual, American Institute of Steel Construction, 2005.
[27] Eurocode 3: Design of steel structures, European Committee for Standardization (CEN), Brussels., EN 1993-1-1, 2005.
[28] ASTM A36 / A36M-14, Standard Specification for Carbon Structural Steel, ASTM International, West Conshohocken, PA, 2014.
[29] ASTM A370-02, Standard Test Methods and Definitions for Mechanical Testing of Steel Products, ASTM International, West Conshohocken, PA, 2001
[30] A. Beyer, N. Boissonnade, A. Khelil, A. Bureau, Influence of assumed geometric and material imperfections on the numerically determined ultimate resistance of hot-rolled U-shaped steel members, Journal of Constructional Steel Research, 147, 103–115, 2018.
[31] Schafer B., Review: The direct strength method of cold-formed steel member design, Journal of Constructional Steel Research, 64, 766–778, 2008.
[32] Schafer B. and Adany S., Buckling analysis of cold-form steel members using cufsm: conventional and constrained finite strip methods, Proceedings of the 18th International Specialty Conference on Cold-formed Steel Structures, Florida, USA, 2006.
[33] Rex C.O. and Easterling W.S., Behavior and modeling of a bolt bearing on a single plate, Journal of Structural Engineering, 129(6), 792–800, 2003.
[34] Design of Latticed Steel Transmission Structures. ASCE 10-97, American Society of Civil Engineers, 1998.